8-26-2022

Rocket Measurements of Electron Energy Spectra From Earth's Photoelectron Production Layer

Aroh Barjatya
Embry-Riddle Aeronautical University, barjatya@erau.edu

Shantanab Debchoudhury
Embry-Riddle Aeronautical University, debchous@erau.edu

Glyn A. Collinson
NASA Goddard Space Flight Center, The Catholic University of America, G & K Rocket Yards

Alex Glocer
NASA Goddard Space Flight center

Dennis Chornay
NASA Goddard Space Flight Center, University of Maryland

See next page for additional authors

Rocket measurements of electron energy spectra from Earth's photoelectron production layer

Glyn A. Collinson [1,2,3], Alex Glocer [1], Dennis Chornay [1,4], Robert Michell [1], Rob Pfaff [1], Tim Cameron [1], Paulo Uribe [1], Rudy A. Frahm [5], Traci Rosnack [1,6], Chris Pirner [1,7], Ted Gass [8], Jim Clemmons [9], Aroh Barjatya [10], Steven Martin [1,7], Hassanali Akbari [1], Shantanab Debchoudhury [10], Rachel Conway [10], Francis Eparvier [11], Eftyhia Zesta [1], Nikolaos Paschalidis [1]

[1]NASA Goddard Space Flight Center, Greenbelt, Maryland, USA
[2]The Catholic University of America, Washington, District of Columbia, USA
[3]G & K Rocket Yards, Interplanetary Expeditions, Criccieth, Gwynedd, UK
[4]University of Maryland, College Park, MD, USA
[5]Southwest Research Institute, San Antonio, TX, USA
[6]Orbital Sciences Corp., Dulles, VA, USA
[7]ADNET Systems, Inc., Bethesda, MD, USA
[8]NASA Sounding Rocket Operations Contract, NASA Wallops Flight Facility, Wallops Island, VA, USA
[9]University of New Hampshire, Durham, NH, USA
[10]Embry-Riddle Aeronautical University, Daytona Beach, FL, USA
[11]Laboratory for Space and Atmospheric Physics, Boulder, CO, USA

Key Points:

- We present *in-situ* observations from a plasma spectrometer flown on a rocket to 131km in the daytime mid-latitude ionosphere
- The instrument returned calibrated measurements of the energy spectra of pristine photoelectrons near the peak of production
- The N_2 absorption feature and He-II photopeaks were partially resolved. Observations are compared with the GLOW electron model.

Corresponding author: Glyn Collinson, glyn.a.collinson@nasa.gov

This article has been accepted for publication and undergone full peer review but has not been through the copyediting, typesetting, pagination and proofreading process, which may lead to differences between this version and the Version of Record. Please cite this article as doi: 10.1029/2022GL098209.

Abstract

Photoelectrons are crucial to atmospheric physics. They heat the atmosphere, strengthen planetary ambipolar electric fields, and enhance the outflow of ions to space. However, there exist only a handful of measurements of their energy spectrum near the peak of photoproduction. We present calibrated energy spectra of pristine photoelectrons at their source by a prototype Dual Electrostatic Analyzer (DESA) instrument flown on July 11 2021 aboard the *Dynamo-2* sounding rocket (NASA № 36.357). Photopeaks arising from 30.4nm He-II spectral line were observed throughout the flight above 120km. DESA also successfully resolved the rarely observed N_2 absorption feature. Below 10eV observations were in good agreement with the GLOW suprathermal electron. Above 10eV fluxes substantially deviated from the model by as much as an order of magnitude.

Plain Language Summary

We designed, built, and flew a new scientific instrument for the measurement of photoelectrons which are created when sunlight shines on the upper atmosphere. The instrument was launched on a suborbital rocket from NASA Wallops Flight Facility just before 2pm on July 11th 2021. The rocket flew to an altitude of 131 km before splashing down in the Atlantic Ocean 8 mins later. The instrument gathered scientific data during the flight, measuring the energy spectrum of electrons in Earth's ionosphere. Historical observations of electron spectra at these altitudes are extremely rare, and are often uncalibrated and/or not archived. We present calibrated observations of the pristine spectra of Earth's electrons near their source as a reference for future computer modeling and exploration of Earth's ionosphere.

1 Introduction

When sunlight shines upon planetary atmospheres, energetic photoelectrons are excited and ejected from neutral atoms by the absorption of extreme ultraviolet solar radiation. Photoelectrons play a key role in many aspects of atmospheric physics; they are an important source of heat for the ionosphere and upper thermosphere (Shea et al., 1968); they strengthen the ambipolar electric potential drop generated by planetary ionospheres (Lemaire, 1972; Khazanov et al., 1997) which is critical to understanding the quiet time polar wind (Banks & Holzer, 1968) and its global structure (Glocer et al., 2017); photoelectrons are also important in magnetospheric physics, enabling field line tracing (Xu et al., 2017, 2021), and the measurement of planetary electric potentials (Coates et al., 1985, 2015; G. A. Collinson et al., 2016, 2017).

While photoelectrons are crucial to our understanding of Earth's ionosphere, they are produced at altitudes that are extremely challenging to explore *in-situ* (Lee et al., 1980). Photoproduction peaks at approximately 130 km (see Fig. 1), too high for aircraft and balloons, but too low for satellites to reach without propulsion to prevent reentry. There is thus a paucity of observations from the peak of the photoproduction layer with which to compare with theoretical models. At Mars the photoproduction is accessible to satellites due to the thinner atmosphere (Coates et al., 2011). However, recent observations by the Mars Atmosphere and Volatile Evolution (MAVEN) mission have not been consistent with current models of photoelectron thermalization, suggesting that electron thermalization processes in planetary thermospheres are not well understood quantitatively (Peterson, 2021).

The energy spectra of photoelectrons is very complex. Photoelectrons exhibit multiple sharp peaks from solar emission lines and a sudden drop off at ∼60 eV due to a cutoff in the solar spectrum near 16 nm (Nagy & Banks, 1970; Mantas & Hanson, 1979). Earth's photoelectrons also exhibit a trough in electron flux at around 2.5 eV resulting from the absorption of photoelectron kinetic energy via the collisional excitation of the

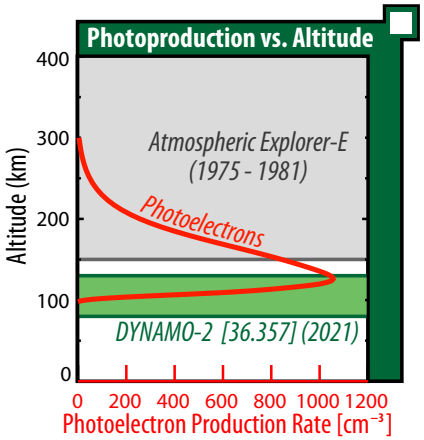

Figure 1. Photoelectron production as a function of altitude in the dayside ionosphere according to calculations using the GLOW superthermal electron model

N_2 vibrational mode (Nisbet, 1968). This trough-like N_2 absorption feature is fundamentally unstable in space plasmas (which left alone naturally prefer to decay towards a maxwell-boltzman distribution) and must constantly be maintained through continuous collisional excitation with N_2 molecules. While the N_2 feature can be consistently observed near to the photoproduction source, it disappears at altitudes above ∼265 km - 300 km (depending on local zolar zenith angle) (Lee et al., 1980). Only a handful of measurements of the N_2 absorption feature have ever been reported (Doering et al., 1976; Lee et al., 1980). The low energy of this feature makes it additionally challenging to measure since 1.) the gyroradius of these electrons (≈10 cm) approaches the size of most spectrometers, and 2.) measurements at these low energies can easily be contaminated by electrons originating from either the spacecraft or the sensor itself (Peterson, 2021).

The energy spectra of photoelectrons was measured from orbit by Atmospheric Explorer-C (Peterson et al., 1977) and then by Atmospheric Explorer-E (AE-E) (Doering et al., 1976; Peterson et al., 1977; Lee et al., 1978, 1980; Jasperse & Smith, 1978). However, these spacecraft could only study the topside of the photoproduction region (Fig. 1) where the energy spectrum has evolved with increasing altitude due to electron-electron collisions, transport, and physical instabilities. Also, the best of our knowledge, these data were not archived in sufficient resolution to resolve fine spectral features such as the individual photopeaks or the N_2 feature.

Apart from the topside measurements by AE-E (Lee et al., 1980), only a handful of rocket missions have successfully returned data from the photoproduction region [e.g. Hinteregger (1960); Shea et al. (1968); Doering et al. (1970)], however very few have successfully observed the low-energy N_2 absorption feature. Hays and Sharp (1973) built a hyperbolic electrostatic analyzer that was specifically designed as a low-energy Photoelectron Spectrometer. They launched it on NASA sounding rocket № 13.051 on February 8th, 1971, from the White Sands Missile Range, to an altitude of 265 km. While the instrument resolved the N_2 absorption feature, the launch occurred just past dawn, and thus much of the flight were under effectively night-time conditions and not representative of the main dayside photoproduction region. McMahon and Heroux (1978) launched a cylindrical electrostatic analyzer aboard a rocket (also from White Stands) on February 28, 1976. This mission successfully resolved the N_2 absorption feature near local noon, but their instrument was not calibrated, and thus the fluxes reported were all relative and not absolute.

Here we present new calibrated observations from near the peak of Earths photoproduction region from an experimental plasma analyzer. The observations were made at 130.85 km on a Black Brant XI rocket (NASA № 36.357 *Dynamo-2*) launched from NASA's Wallops Flight Facility on July 11th 2021 at 17:56 GMT (13:56 local time). The instrument, called the Dual Electrostatic Analyzer (DESA), successfully measured the energy spectra of photoelectrons between 0.5 eV and 1keV at an energy resolution of 16 % ΔE/E. This paper is organized as follows. In section 2 we describe the DESA sensor and its performance. In section 3 we give an overview of the flight of DESA aboard *Dynamo-2*. In section 4 we present the results from the flight. Finally, in section 5 we summarize the results and our conclusions.

2 The Dual Electrostatic Analyzer (DESA) Instrument

2.1 *Dynamo-2* DESA objectives

DESA is a new type of plasma analyzer that has been specifically designed to measure the energy spectrum of electrons near planetary bodies. Eight DESA sensors flew recently (May 11th 2022) aboard NASA's *Endurance* rocket mission (G. Collinson et al., 2022) (NASA № 47.001). Another DESA sensor is manifested to fly on NASA's 6U *Dione* cubesat. In order to gain invaluable flight experience prior to these missions, a prototype sensor (serial number DESA-NX-02A, Fig 2b) was flown as a hosted payload aboard one of the two *Dynamo-2* rockets (NASA № 36.357).

Prior to launch, *Dynamo-2* was predicted to reach apogee somewhere between 121 km (2σ low) and 148 km (2σ high). Should the rocket fly low, it could have fallen just short of entering the photoproduction layer, in which case DESA may not have returned useful scientific data. Thus, the primary objective of the *Dynamo-2* DESA experiment was to gather engineering data and evaluate the performance of its novel optics and new electronics in spaceflight.

However, should *Dynamo-2* fly high, or even just attain its nominal apogee (135 km), then this would put it near the peak of the photoproduction region. Thus, the DESA-NX-02A sensor was configured as a very low-energy (0.5eV - 1keV) photoelectron spectrometer in the hopes of achieving a secondary objective of measuring the energy spectra of electrons near the photoproduction peak, with a tertiary objective of attempting to resolve the seldom-seen N_2 absorption feature.

2.2 DESA Sensor Description

2.2.1 Hybrid Optics

DESA is a new kind of hybrid plasma spectrometer, the full operational principal of which is described by G. A. Collinson et al. (2018). Figure 2a shows a cross-section through the prototype flown aboard *Dynamo-2*. Electrons entering DESA (Fig. 2a) first traverse a "Top Hat" electrostatic analyzer (ESA) (Carlson et al., 1982). The ESA provides an initial broad bandpass energy filter to incoming electrons, and scans over the full energy range (0.5 eV to 1keV) in logarithmic steps. Electrons then pass through a high-resolution Retarding Potential Analyzer (RPA). This feature of the instrument was not used for the purposes of this study, and all data shown were taken with the RPA grounded and functioning purely as a beam guide.

Simulations of the response of top hat analyzers to magnetic fields by Clark et al. (2016) showed that as long as the magnetic field is aligned with the aperture (and incident flux of plasma), then the energy selection of a top-hat analyzer is unaffected. DESA optics have been designed to use this inherent property of top hat ESAs to correctly measure the energy of electrons down to 0.5eV without the need for magnetic shielding, as long as its aperture/boresight is aligned with the magnetic field. The only caveat is that

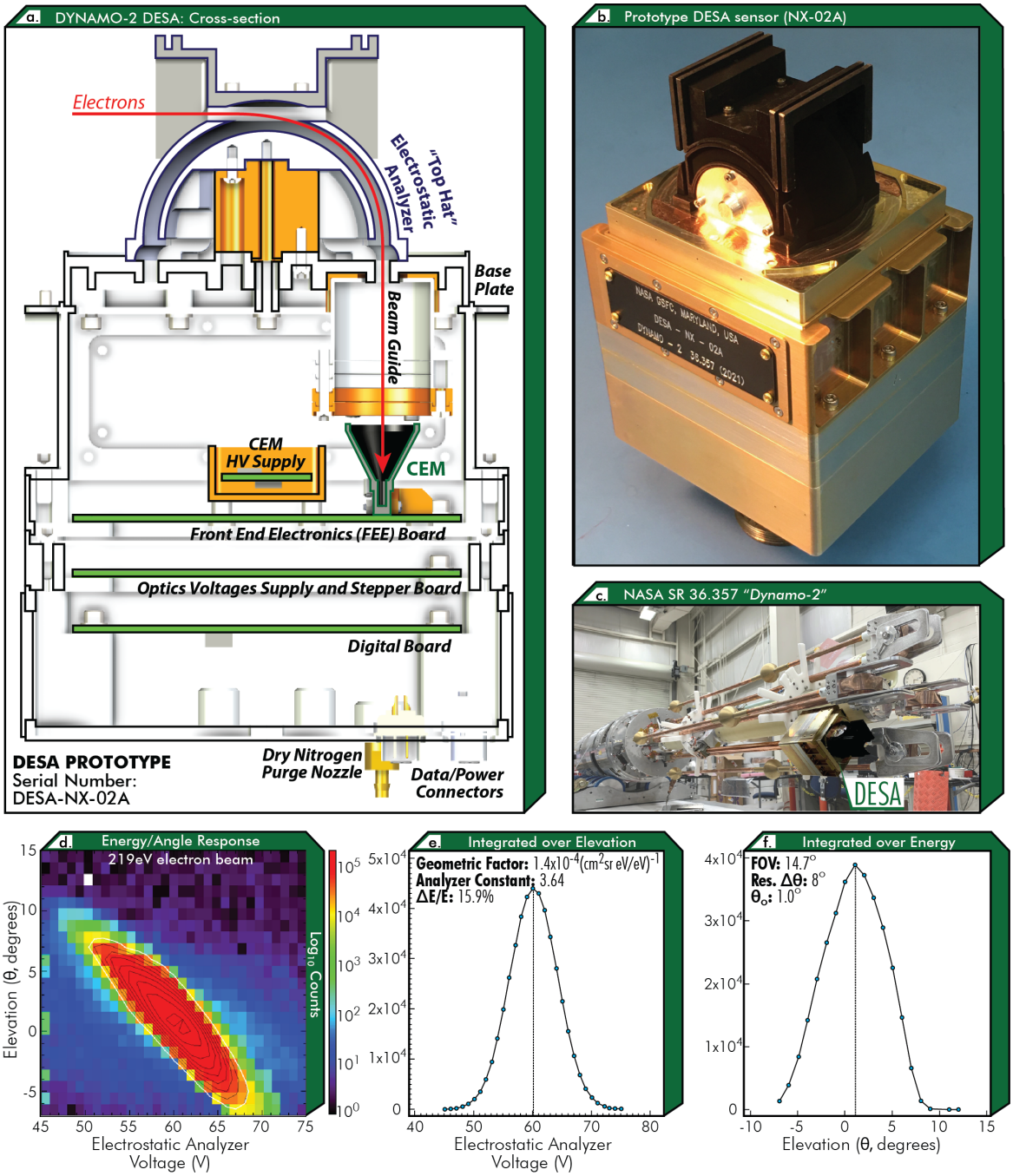

Figure 2. The Dual Electrostatic Analyzer (DESA) experiment: a.) Cross-section of DESA sensor showing main components; b.) photograph of the prototype DESA sensor (serial number NX-02A) just prior to delivery; c.) Photograph of DESA-NX-02A mounted on the Dynamo-2 rocket (NASA № 36.357). Bottom three panels show calibration data from the sensor; d.) Variation in counts as a function of elevation angle and voltage on the electrostatic analyzer; e.) Energy response; f.) Elevation Response.

Earth's magnetic field twists the path of incoming electrons as they pass through the ESA (as per Clark et al. (2016)). Thus, while DESA can measure down to 0.5eV in energy, these electrons are coming from an azimuthal angle of as much as 20° in azimuth (out of the page with respect to Fig. 2a), depending on the energy of the electrons and the local magnetic field strength. This was not an issue for this flight to the photoproduction layer where the electron population under study should be close to isotropic.

2.2.2 Electron detection

Having traversed the optics, electrons fall into a Channel Electron Multiplier (CEM) which creates an avalanche of charge with a gain of $\approx 1 \times 10^8$. This pulse of charge is amplified, then goes through a discriminator after which a count is registered. DESA is designed to accommodate two CEMs, so that the instrument may simultaneously measure electrons from two opposing directions (field aligned and anti-aligned). However, on this test flight, only one CEM was flown. The housing of the sensor included a nozzle for the hook-up of a dry nitrogen purge line to keep the inside of the sensor (and the CEM) dry when the DESA sensor was being integrated with the rocket on the ground. Operation of high voltage charge amplifiers at low altitudes brings the risk of electrostatic high-voltage breakdown. To attempt to minimize this risk, DESA was left off until the spacecraft passed 120 km in altitude using a pre-programmed timer. DESA then gathered good data from that point through apogee (131 km) and for the entire downleg until below 90 km on re-entry.

2.2.3 Support electronics

The DESA NX-02A sensor head has three electronics boards. The Front End Electronics (FEE) board includes mounting space for two CEMs, two pulse amplifier and discriminator circuits, and a daughter board containing a 3kV HV supply for the CEMs (potted inside a shielded box). Below this is a board which generates and regulates the voltages on the optics. At the bottom of the sensor is a digital card containing an FPGA which controls the FEE and stepper board and sends out counts and housekeeping data. Finally, the DESA sensor is supported by a main electronics box mounted to the body of the rocket which provides the regulated low voltages required by the sensor and feeds its data into the rocket's telemetry system.

2.2.4 Accommodation

The prototype DESA-NX-02A sensor was mounted on the end of a short ∼50cm fiberglass hinged boom (Fig. 2c) to get it as far outside the contaminating plasma-sheath of the rocket as possible. For a $1.37 \times 10^6 cm^{-3}$, 525 K thermal plasma at 131 km the electron debeye length (and thus the approximate thickness of the sheath) is 0.43 cm. The 50 cm length of the boom enabled DESA to measure electrons up to ∼48 eV without being impinged by the spacecraft body by gyroradius effects. The boom was wrapped in copper tape to be conductive and at the same potential as the skin of the sensor and spacecraft. *Dynamo-2* was a spinning spacecraft, whose spin-axis was physically aligned to the magnetic field during flight by the on-board attitude control system. The DESA sensor was mounted so that its aperture would align with the spin axis, and hence the ambient magnetic field. The single working aperture was pointed upwards to look towards space after deployment.

The DYNAMO-2 main spacecraft included a Swept Langmuir Probe (SLP) which for the purposes of this study was used to measure the electrical potential difference between the ionospheric plasma and the spacecraft. Effectively identical to that flown on the DYNAMO-1 mission (Pfaff et al., 2020), this SLP was mounted on the spin-axis of the spacecraft. The VxB electric fields of $40-50 mV/m$ encountered during this experiment due to the rocket's motion across the ambient magnetic field direction would re-

sult in small voltage variations of $\pm 20 - 25mV$ (varying sinusoidally with the payload spin period of ≈2 seconds) at the DESA location which would produce very small changes to the DESA applied voltages. The chassis of the DESA sensor was electrically grounded to the main spacecraft, and hence, would be at the same reference potential as the Langmuir probe.

2.3 Calibration

The DESA-NX-02A sensor was calibrated at NASA Goddard Space Flight Center in the same facility as the Fast Plasma Investigation for the Magnetospheric Multiscale Mission (Pollock et al., 2016). Figure 2d shows an Energy/Angle plot of the counts detected as a function of the voltage on the electrostatic analyzer and elevation angle. Following G. A. Collinson et al. (2012), this data product was used to calculate a geometric factor of the instrument of $1.4{\times}10^{-4}(cm^2\, sr\, eV/eV)^{-1}$. By integrating this scan over all elevations, we find that DESA has a gaussian energy acceptance bandpass (fig. 2e, typical for a top hat analyzer) with an analyzer constant (energy sampled divided by voltage applied to ESA) of 3.64, and energy resolution of $15.9\%\Delta E/E$. DESA has a fixed field of view of 14.7° elevation (fig. 2f) by 17.8° in azimuth (not shown for brevity).

3 Overview of the 36.357 *Dynamo-2* Mission

Dynamo-2 (NASA №36.357) launched from NASA's Wallops Island Flight Facility, Wallops Island, VA at 17:56:00 Greenwich Mean Time (GMT) on July 11th 2021 (local time of 13:56:00). The payload was launched on a two stage solid-fueled Black Brant IX launch vehicle, with a Terrier booster stage to lift it off the launch pad (Fig. 3a), and a Black Brant main stage to lift it to space. The nosecone was jettisoned at 17:57:28 GMT (at approximately 75 km on the upleg), with the DESA boom successfully deploying 2s later and locking into its flight configuration (boom at 90° to the payload spin-axis).

An on-board timer powered the DESA-NX-02A sensor 151.14 s after launch at an altitude of 122.4 km on the up-leg. Fig. 3b shows the altitude above sea level of 36.357 *Dynamo-2* during DESA operation. Apogee was at 130.85 km at 17:59:14 GMT (1:59:14 ET local time). DESA continued to be fully functional until an altitude of ∼ 88 km on re-entry, at which point the rising air pressure caused high-voltage breakdown. The rest of the sensor continued to function for nearly a minute until the spacecraft hit the bulk of the atmosphere and all data ceased. Around 18:04:12 GMT, the *Dynamo-2* payload impacted the Atlantic Ocean near 36.627°N, 72.550°W, coming to rest in approximately 3,480m of water.

4 Results

DESA operated in multiple interleaved modes over an ∼8 second duty cycle consisting of 157 voltage steps on the optics. This study focuses on only the 52 steps associated with the operation of the ESA which returned useful science data. We shall first present an overview of all data collected in this mode and then focus on the four cleanest spectra taken near to apogee.

4.1 Data Overview: Time vs. Energy Electron Spectrogram

Fig. 3c shows a time-energy spectrogram of DESA observations, whereby the color denotes log_{10} of differential energy flux. These data have been calibrated from raw counts into flux. The final correction of these spectra for spacecraft potential will be discussed shortly. Three features are prominent in the DESA spectrogram. Firstly, a narrow band of electron emission near ≈20eV with fluxes peaking at $\sim 1{\times}10^7 eV(cm^2\, s\, sr\, eV)^{-1}$. This is extremely consistent with the cluster of photopeaks expected from photoinization of

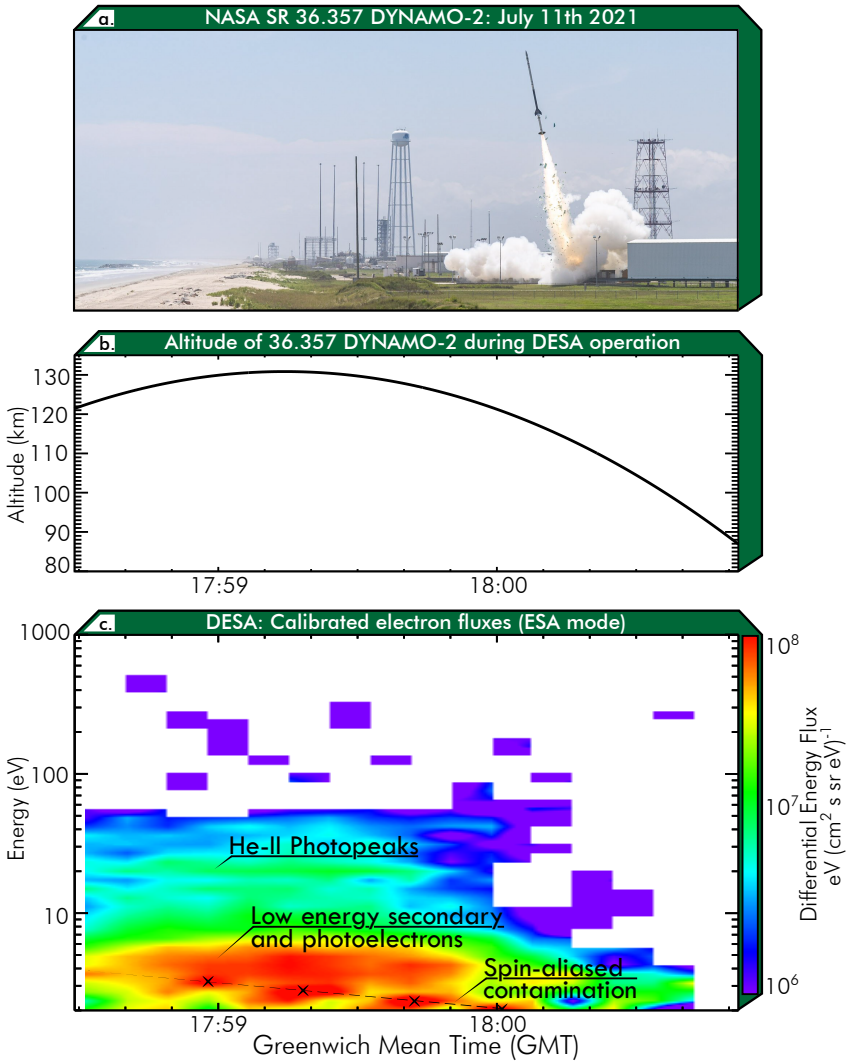

Figure 3. a.) Launch of 36.357 *Dynamo-2* (NASA Wallops/Allison Stancil); b.) Altitude of 36.357 during DESA operation; c.) Calibrated electron fluxes, uncorrected for background counts or spacecraft potential

oxygen and nitrogen by the bright He-II 30.4nm solar emission line (Doering et al., 1976; Lee et al., 1980; Coates et al., 1985). The photopeaks were observed immediately upon switch-on of the instrument at 122 km, and were clearly observed throughout the flight until the rocket descended back below ∼120 km. A broader population of superthermal electrons was also observed near ≈4eV. This bulk population of low energy electrons is an admixture of secondary electron production, photoproduction, and electron cascading from higher to lower energies through collisions (Khazanov, 2010).

Also occasionally visible at low energies (<4 eV) was contamination from photoelectrons generated inside the instrument. The spinning of the rocket caused light to strobe off and on inside the sensor, with the most contamination being observed when DESA was at a roll angle of ±90°. We posit that it was at these angles that sunlight could illuminate the inside of the ESA, resulting in photoemission from its metal surfaces. The 8.0 s duty cycle of the instrument was almost, but not quite, in phase with the 2.14 s spin rate (0.47 Hz) of the rocket, and thus in the time it took for DESA to be rotated back to an angle where it would be contaminated, the instrument hadn't quite reached the same point in its stepper table. The result is that the contamination appears in progressively lower energy bins over the flight in fig 3c.

This spin-aliased energy-dependent contamination is challenging to separate automatically and the best approach for further analysis is to examine each scan individually.

4.2 Examination of spectra measured near Apogee

Figure 4 shows the 4 scans of DESA-NX-02A which were least contaminated, which fortuitously occurred around apogee.

4.2.1 Spacecraft potential correction

The dashed dark blue lines on Fig. 4 show the same calibrated (but uncorrected) data as Fig. 3c. Using measurements from a swept Langmuir Probe carried aboard 36.357 *Dynamo-2*, the potential difference between the spacecraft and ambient plasma was calculated for each of these sweeps. These spectra were then corrected for this potential using Louiville's theorem (converting through phase space density). For a full description of this technique, see e.g. G. A. Collinson et al. (2016), supplemental materials S1.

4.2.2 Identification of possibly contaminated datapoints

Ideally, the background contamination due to photoelectrons generated inside DESA would be completely removed from these spectra before calibration. However, this is challenging for the Dynamo-2 flight. Firstly, secondary/photoelectrons have a natural energy dependance, and so the amount of contamination naturally varies from one energy bin to the next. Secondly, as mentioned above, the amount of contamination varied greatly over the 2.14 s spin of the rocket as the sun strobed off and on inside the instrument, with most contamination at roll angles $> \pm 90°$. It is thus difficult to reliably subtract these spikes in internal photoelectron contamination, since it is not a constant value or simple function.

However, to identify which datapoints are more likely to be contaminated by photoelectrons generated inside the DESA sensor, the calibrated and corrected data product was then separated into two; (1) Periods when the DESA sensor was at a roll angle $< \pm 90°$ represent the best quality data that are the least likely to be contaminated (thick dark blue, Fig. 4); (2) roll angle $> \pm 90°$ and thus more likely to be contaminated (light blue line, Fig. 4). However, it is key to stress that the data points labeled "more" reliable (dark blue) are still likely to be contaminated to some extent. Photoelectron con-

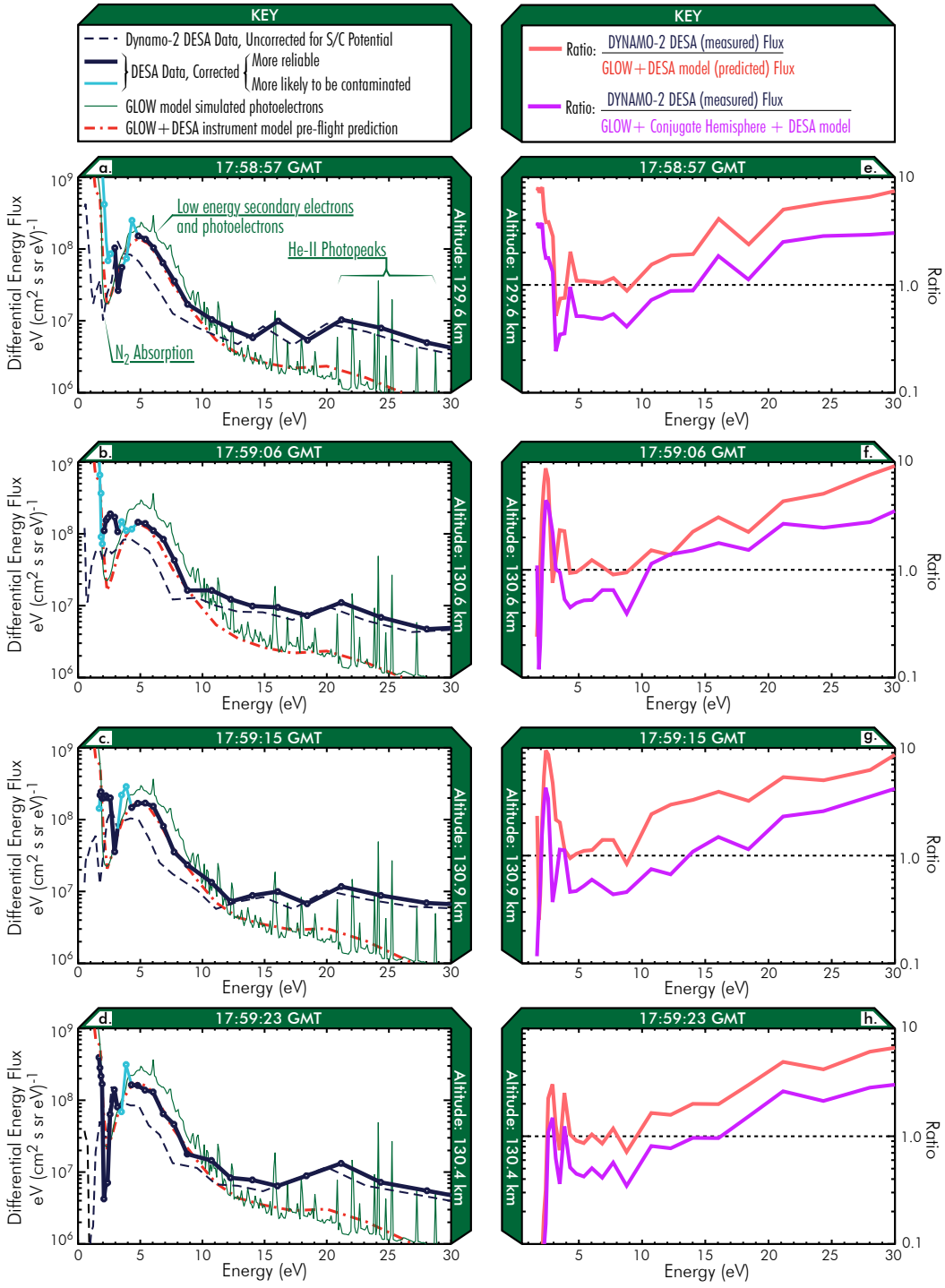

Figure 4. (a-d) Calibrated electron spectra from near apogee, corrected for spacecraft potential from the Dynamo-2 langmuir probe. The DESA sensor successfully resolved and measured several key spectral features that are predicted by models. (e-h) Ratio of flux measured during the flight to that predicted by the GLOW model / instrument model

tamination was most predominant below 5 eV, and thus measurements above this energy are colored in dark blue (least contaminated).

4.2.3 Comparison of DESA results to GLOW model prediction

For direct comparison with flight data, the GLOW simulations were put through an instrument simulator which mimics the Gaussian response function of the DESA-NX-02A ESA (fig 2f) to create a synthetic data product (red dashed line, Fig. 4a-d).

Figs. 4e-h show the ratio between the flux measured by DESA to that predicted by the combined GLOW + instrument models (orange line). Below ∼10eV observations were are generally consistent with the prediction. In particular, the fluxes and overall shape of the low energy population of secondary and photoelectrons are in generally good agreement (mean ratio 1.62 ± 0.3 between 3 eV to $\approx$ 10 eV). Below 3eV, the ratio deviates from 1 by up to an order of magnitude due to the above-described contamination in the sensor from photoelectrons generated internally within DESA.

Between 10eV and 30eV, measured fluxes diverge from GLOW by up to an order of magnitude. One explanation for this may be that DESA is also observing photoelectrons from an additional source in the magnetically conjugate southern hemisphere (Peterson et al., 1977), (Solomon et al., 2020). In order to make a first-order estimate of this additional contribution of photoelelectrons we repeated the GLOW simulations, taking the upward fluxes at the top of the model and using them to set the downward flux. This downward flux was multiplied by a plasmaspheric transparency factor which was crudely estimated to be 20% for energies below 20eV, 30% for energies between 20 and 30eV, and 40% for energies above 30eV. The solution was iterated until convergance was achieved. The purple line in Figs. 4e-h shows the ratio of the data to the model with this additional source of conjugate hemisphere photoelectrons. In general, we find the comparison improves distinctly in the tail of the distribution (>9 eV). However, the agreement at lower energies is worse. For now we can only conclude that conjugate photoelectrons may resolve some of the discrepancy above 9 eV, but more detailed studies would be needed to include this effect at lower energies.

A second explanation might be that uncertainties ionization cross sections and incoming photon flux may contribute to the discrepancies between the data and model. This is a prime topic for analysis of measurements by the 8 DESA sensors of the recently launched *Endurance* rocket (G. Collinson et al., 2022).

4.2.4 Likely detection of N_2 Absorption feature

All four scans show evidence of erosion in flux near $3eV$, corresponding to the N_2 absorption feature observed by AE-E and previous rockets (Peterson et al., 1977; Hays & Sharp, 1973; McMahon & Heroux, 1978; Lee et al., 1980). However, to our knowledge, these are the first calibrated measurements of this feature from near the peak of the photoproduction region. The N_2 absorption feature was best resolved in the scan (Fig. 4d), taken just after apogee. DESA measurements reveal that the drop in electron flux is sharper than predicted by the GLOW model, with a reduction in flux of nearly 2 orders of magnitude at 2.5eV.

4.2.5 Detection of He-II Photopeaks

All four scans exhibit a peak in flux near 22 eV associated with the He-II photopeaks (as Fig. 3c). DESA is unable to resolve the individual peaks with the 16% $\Delta E/E$ resolution of its ESA alone. The result is a single merged peak which has been observed at planetary ionospheres throughout the solar system [e.g. Coates et al. (2015)]. The en-

ergy of the observed peak diverges from that in the GLOW+Instrument model, strongly motivating future model/data comparisons with the *Endurance* DESA dataset.

5 Summary and Conclusions

We present new observations of the energy spectra of superthermal electrons from near the peak of Earth's photoelectron production layer. Data from this region is extremely rare, being too high for aircraft but too low for satellites. Thus, there exist only a handful of past rocket-borne observations, none of which are archived and/or calibrated and corrected for spacecraft potential.

The new measurements were made by a prototype for the new series of Dual Electrostatic Analyzer (DESA) instruments. The sensor (serial number DESA-NX-02A) was flown aboard NASA's 36.357 *Dynamo-2* rocket, launching from NASA's Wallops Flight Facility on July 11th 2021 near 2pm local time.

Apogee was at 130.85km, near the peak of photoelectron production where DESA successfully measured several hallmark spectral features. The He-II photopeaks were detected as a single merged peak throughout the flight when above 120km. For the first time in over 40 years DESA successfully resolved the 2.5eV N_2 absorption feature, for which we only have a handful of previous measurements, and never before a fully calibrated measurement in the peak of the source region.

Measurements below 3eV were heavily contaminated by photoelectrons produced inside the sensor. This was challenging to subtract on this flight as the degree of contamination was dependent not only on energy but also with the roll of the rocket. In response to this, subsequent DESA sensors feature a light-tight cover over their optics and a mode to measure contamination as a function of energy.

There was generally good agreement between *DYNAMO-2* DESA measurements and the GLOW superthermal electron model below $\sim$ 10 eV for the bulk population of secondary electrons and photoelectrons (Khazanov, 2010). Above $\sim$ 10 eV, measured fluxes diverged from the GLOW model began to substantially deviate, with an order of magnitude higher fluxes at 30eV than predicted. Investigating this disparity is a prime topic for analyzing data from the DESAs aboard the *Endurance* rocket (NASA № 47.001) (G. Collinson et al., 2022). The engineering lessons learned from *Dynamo-2* enabled future DESA sensors to have higher resolution, improved signal to noise, and less contamination.

Open Research

Dynamo-2 DESA data is avaliable at `https://spdf.gsfc.nasa.gov/pub/data/aaa_sounding_rockets/dynamo2/` and `https://cdaweb.gsfc.nasa.gov/pub/data/aaa_sounding_rockets/dynamo2/`.

Acknowledgments

This study was supported by NASA's Heliophysics Technology and Instrument Development for Science (H-TIDeS) program, by NASA's *Endurance* rocket mission (grant № 80NSSC19K1206) and the Dynamo-2 mission. The DESA instrument was developed through the Goddard Space Flight Center Internal Research And Development (IRAD) program. We would also like to thank Dr. S. Solomon for making the GLOW model available.

References

Banks, P. M., & Holzer, T. E. (1968, November). The polar wind. *J. Geophys. Res.*,

73, 6846-6854. doi: 10.1029/JA073i021p06846

Carlson, C. W., Curtis, D. W., Paschmann, G., & Michel, W. (1982). An instrument for rapidly measuring plasma distribution functions with high resolution. *Advances in Space Research*, *2*, 67-70. doi: 10.1016/0273-1177(82)90151-X

Clark, G., Allegrini, F., McComas, D. J., & Louarn, P. (2016, June). Modeling the response of a top hat electrostatic analyzer in an external magnetic field: Experimental validation with the Juno JADE-E sensor. *Journal of Geophysical Research (Space Physics)*, *121*(6), 5121-5136. doi: 10.1002/2016JA022583

Coates, A. J., Johnstone, A. D., Sojka, J. J., & Wrenn, G. L. (1985, November). Ionospheric photoelectrons observed in the magnetosphere at distances up to 7 earth radii. *Planet. Space. Sci.*, *33*, 1267-1275. doi: 10.1016/0032-0633(85)90005-4

Coates, A. J., Tsang, S. M. E., Wellbrock, A., Frahm, R. A., Winningham, J. D., Barabash, S., ... Crary, F. J. (2011, August). Ionospheric photoelectrons: Comparing Venus, Earth, Mars and Titan. *Planet. Space. Sci.*, *59*, 1019-1027. doi: 10.1016/j.pss.2010.07.016

Coates, A. J., Wellbrock, A., Waite, J. H., & Jones, G. H. (2015, June). A new upper limit to the field-aligned potential near Titan. *Geophys. Res. Lett.*, *42*(12), 4676-4684. doi: 10.1002/2015GL064474

Collinson, G., Glocer, A., Pfaff, R., Barjatya, A., Bissett, S., Blix, K., ... Wilson, T. (2022, August). The Endurance Rocket Mission. *Space Sci. Rev.*, *218*(5), 39. doi: 10.1007/s11214-022-00908-0

Collinson, G. A., Chornay, D. J., Glocer, A., Paschalidis, N., & Zesta, E. (2018, November). A hybrid electrostatic retarding potential analyzer for the measurement of plasmas at extremely high energy resolution. *Review of Scientific Instruments*, *89*(11), 113306. doi: 10.1063/1.5048926

Collinson, G. A., Dorelli, J. C., Avanov, L. A., Lewis, G. R., Moore, T. E., Pollock, C., ... Adrian, M. L. (2012, March). The geometric factor of electrostatic plasma analyzers: A case study from the Fast Plasma Investigation for the Magnetospheric Multiscale mission. *Review of Scientific Instruments*, *83*(3), 033303.

Collinson, G. A., Frahm, R., Glocer, A., Coates, A. J., Grebowsky, J. M., Barabash, S., ... Zhang, T. L. (2016, June). The electric wind of Venus: A global and persistent "polar wind"-like ambipolar electric field sufficient for the direct escape of heavy ionospheric ions. *Geophys. Res. Lett.*. doi: 10.1002/2016GL068327

Collinson, G. A., Mitchell, D., Xu, S., Glocer, A., Grebowsky, J., Hara, T., ... Jakosky, B. (2017, February). Electric Mars: A large trans-terminator electric potential drop on closed magnetic field lines above Utopia Planitia. *Journal of Geophysical Research (Space Physics)*, *122*, 2260-2271. doi: 10.1002/2016JA023589

Doering, J. P., Fastie, W. G., & Feldman, P. D. (1970, January). Photoelectron excitation of N_2 in the day airglow. *J. Geophys. Res.*, *75*(25), 4787. doi: 10.1029/JA075i025p04787

Doering, J. P., Peterson, W. K., Bostrom, C. O., & Potemra, T. A. (1976, March). High resolution daytime photoelectron energy spectra from AE-E. *Geophys. Res. Lett.*, *3*, 129-131. doi: 10.1029/GL003i003p00129

Glocer, A., Khazanov, G., & Liemohn, M. (2017). Photoelectrons in the quiet polar wind. *Journal of Geophysical Research: Space Physics*, *122*(6), 6708–6726. Retrieved from `http://dx.doi.org/10.1002/2017JA024177` (2017JA024177) doi: 10.1002/2017JA024177

Hays, P. B., & Sharp, W. E. (1973, January). Twilight airglow: 1. Photoelectrons and [O I] 5577-Angstrom radiation. *J. Geophys. Res.*, *78*(7), 1153. doi: 10.1029/JA078i007p01153

Hinteregger, G. E. (1960, January). Combined retarding potential analysis of photo-

electrons and environmental charged particles up to 234 km. In *Space research* (p. 304).

Jasperse, J. R., & Smith, E. R. (1978, October). The photoelectron flux in the Earth's ionosphere at energies in the vicinity of photoionization peaks. *Geophys. Res. Lett.*, *5*(10), 843-846. doi: 10.1029/GL005i010p00843

Khazanov, G. V. (2010). *Kinetic Theory of the Inner Magnetospheric Plasma* (Vol. 372). New York, NY: Springer Science & Business Media.

Khazanov, G. V., Liemohn, M. W., & Moore, T. E. (1997, April). Photoelectron effects on the self-consistent potential in the collisionless polar wind. *J. Geophys. Res.*, *102*, 7509-7522. doi: 10.1029/96JA03343

Lee, J. S., Doering, J. P., Bostrom, C. O., & Potemra, T. A. (1978, July). Measurement of the daytime photoelectron energy distribution from AE-E with improved energy resolution. *Geophys. Res. Lett.*, *5*(7), 581-583. doi: 10.1029/GL005i007p00581

Lee, J. S., Doering, J. P., Potemra, T. A., & Brace, L. H. (1980, October). Measurements of the ambient photoelectron spectrum from atmosphere explorer: I. AE-E measurements below 300 km during solar minimum conditions. *Planet. Space. Sci.*, *28*(10), 947-971. doi: 10.1016/0032-0633(80)90058-6

Lemaire, J. (1972). Effect of escaping photoelectrons in a polar exospheric model. *Space Research XII*, *12*, 1413-1416.

Mantas, G. P., & Hanson, W. B. (1979, February). Photoelectron fluxes in the Martian ionosphere. *J. Geophys. Res.*, *84*, 369-385. doi: 10.1029/JA084iA02p00369

McMahon, W. J., & Heroux, L. (1978, April). Rocket measurement of thermospheric photoelectron energy spectra. *J. Geophys. Res.*, *83*(A4), 1390-1394. doi: 10.1029/JA083iA04p01390

Nagy, A. F., & Banks, P. M. (1970, November). Photoelectron fluxes in the ionosphere. *J. Geophys. Res.*, *75*(31), 6260-6270. doi: 10.1029/JA075i031p06260

Nisbet, J. S. (1968, January). Photoelectron escape from the ionosphere. *Journal of Atmospheric and Terrestrial Physics*, *30*(7), 1257-1278. doi: 10.1016/S0021-9169(68)91090-8

Peterson, W. K. (2021, April). Perspective on energetic and thermal atmospheric photoelectrons. *Frontiers in Astronomy and Space Sciences*, *8*, 41. doi: 10.3389/fspas.2021.655309

Peterson, W. K., Doering, J. P., Potemra, T. A., McEntire, R. W., & Bostrom, C. O. (1977, March). Conjugate photoelectron fluxes observed on Atmosphere Explorer C. *Geophys. Res. Lett.*, *4*, 109-112. doi: 10.1029/GL004i003p00109

Pfaff, R., Larsen, M., Abe, T., Habu, H., Clemmons, J., Freudenreich, H., ... Angelopoulos, V. (2020, August). Daytime Dynamo Electrodynamics With Spiral Currents Driven by Strong Winds Revealed by Vapor Trails and Sounding Rocket Probes. *Geophys. Res. Lett.*, *47*(15), e88803. doi: 10.1029/2020GL088803

Pollock, C., Moore, T., Jacques, A., Burch, J., Gliese, U., Saito, Y., ... Zeuch, M. (2016, March). Fast Plasma Investigation for Magnetospheric Multiscale. *Space Sci. Rev.*, *199*, 331-406. doi: 10.1007/s11214-016-0245-4

Shea, M. F., Sharp, R. D., & McElroy, M. B. (1968, January). Measurements and interpretation of low-energy photoelectrons. *J. Geophys. Res.*, *73*(13), 4199. doi: 10.1029/JA073i013p04199

Solomon, S. C., Andersson, L., Burns, A. G., Eastes, R. W., Martinis, C., McClintock, W. E., & Richmond, A. D. (2020, March). Global-Scale Observations and Modeling of Far-Ultraviolet Airglow During Twilight. *Journal of Geophysical Research (Space Physics)*, *125*(3), e27645. doi: 10.1029/2019JA027645

Xu, S., Frahm, R. A., Ma, Y., Luhmann, J. G., & Mitchell, D. L. (2021, October). Magnetic Topology at Venus: New Insights Into the Venus Plasma Environment. *Geophys. Res. Lett.*, *48*(19), e95545. doi: 10.1029/2021GL095545

Xu, S., Mitchell, D., Liemohn, M., Fang, X., Ma, Y., Luhmann, J., ... Jakosky, B. (2017, February). Martian low-altitude magnetic topology deduced from MAVEN/SWEA observations. *Journal of Geophysical Research (Space Physics)*, *122*, 1831-1852. doi: 10.1002/2016JA023467